J|A|C|S
ARTICLES
Published on Web 04/26/2002

Solid-State ^{67}Zn NMR Spectroscopy in Bioinorganic Chemistry. Spectra of Four- and Six-Coordinate Zinc Pyrazolylborate Complexes Obtained by Management of Proton Relaxation Rates with a Paramagnetic Dopant

Andrew S. Lipton,[†] Terri A. Wright,[‡] Michael K. Bowman,[†] Daniel L. Reger,[‡] and Paul D. Ellis*,[†]

Contribution from the Macromolecular Structure & Dynamics Directorate, WR Wiley Environmental Molecular Sciences Laboratory, Pacific Northwest National Laboratory, Richland, Washington 99352, and Department of Chemistry and Biochemistry, University of South Carolina, Columbia, South Carolina 29208

Received December 14, 2001. Revised Manuscript Received February 22, 2002

Abstract: Solid-state ^{67}Zn NMR spectra of model compounds for metalloproteins, such as $[H_2B(3,5\text{-}Me_2pz)_2]_2Zn$ (pz denotes pyrazolyl ring), have been obtained using low temperatures (10 K) to enhance the Boltzmann factor in combination with cross polarization (CP) from ^{1}H to ^{67}Zn. Attempts to observe spectra of other model compounds, such as $[H_2B(pz)_2]_2Zn$, were hindered by long relaxation times of the protons. To decrease the proton relaxation times, the high-spin six-coordinate complex $[HB(3,4,5\text{-}Me_3pz)_3]_2Fe$ has been investigated as a dopant. NMR and EPR measurements have shown that this Fe(II) dopant effectively reduces the ^{1}H spin lattice relaxation time, T_1, of the zinc samples in the temperature range 5−10 K with minimal perturbations of the ^{1}H spin lattice relaxation time in the rotating frame, $T_{1\rho}$. Using this methodology, we have determined the ^{67}Zn NMR parameters of four- and six-coordinate zinc(II) poly(pyrazolyl)borate complexes that are useful models for systems of biological importance. The ^{67}Zn NMR parameters are contrasted to the corresponding changes in the ^{113}Cd NMR parameters for the analogous compounds. Further, these investigations have demonstrated that a temperature-dependent phase transition occurs in the neighborhood of 185 K for $[HB(3,5\text{-}Me_2pz)_3]_2Zn$; the other poly(pyrazolyl)borate complexes we investigated did not show this temperature-dependent behavior. This conclusion is confirmed by a combination of room-temperature high-field (18.8 T) solid-state ^{67}Zn NMR spectroscopy and low-temperature X-ray methods. The utilization of paramagnetic dopants should enable low-temperature cross polarization experiments to be performed on a wide variety of nuclides that are important in bioinorganic chemistry, for example, ^{25}Mg, ^{43}Ca, and ^{67}Zn.

Introduction

Recently, a general strategy for the NMR observation of half-integer quadrupolar nuclides has been presented[1,2] and applied to the first direct observation of a ^{67}Zn resonance in a zinc-dependent metalloprotein.[3] The strategy entails the utilization of low temperatures (4−25 K) to enhance the Boltzmann factor in combination with cross polarization (CP)[4] from ^{1}H to ^{67}Zn and Fourier transformation of the induced signals resulting from a train of Carr−Purcell Meiboom−Gill echoes.[5,6] The CP experiment transfers ^{1}H magnetization to ^{67}Zn accomplishing several important goals in the process. The ^{67}Zn magnetization is increased by as much as the gyromagnetic ratios for ^{1}H to ^{67}Zn ($\gamma_H/\gamma_{Zn} \approx 16$). Further, the spin lattice relaxation time, T_1, of the ^{1}H nuclei rather than T_1 of the ^{67}Zn determines the rate at which the data can be acquired. However, at low temperatures, <25 K, the ^{1}H T_1 can become significant, approaching many minutes to hours at the lowest temperatures. Therefore, in this strategy it is critical to manage the ^{1}H spin lattice relaxation times in the laboratory and rotating frames, T_1 and $T_{1\rho}$, respectively. The former limits the overall rate in which the experiment can be repeated, and the latter dictates the important aspects of the efficiency of the magnetization transfer from the ^{1}H bath to the rare spin ^{67}Zn nuclide in the rotating frame. In the previous examples,[2,3] rapid rotations of methyl groups present in the systems being investigated were exploited as a means to shorten the ^{1}H T_1.[7] The methyl groups provide a relaxation sink for the remainder of the ^{1}H spin system via their rapid internal rotational motion and efficient spin

* To whom correspondence should be addressed. E-mail: paul.ellis@pnl.gov. Phone: (509)372-3888. Fax: (509)376-2303.
[†] Pacific Northwest National Laboratory.
[‡] University of South Carolina.

(1) Larsen, F. L.; Lipton, A. S.; Jakobsen, H. J.; Nielsen, C. N.; Ellis, P. D. *J. Am. Chem. Soc.* **1999**, *121*, 3783−3784.
(2) Lipton, A. S.; Sears, J. A.; Ellis, P. D. *J. Magn. Reson.* **2001**, *151*, 48.
(3) Lipton, A. S.; Buchko, G. W.; Sears, J. A.; Kennedy, M. A.; Ellis, P. D. *J. Am. Chem. Soc.* **2001**, *123*, 992−993.
(4) Pines, A., Gibby, M. G., Waugh, J. S. *J. Chem. Phys.* **1972**, *56*, 1776.
(5) (a) Carr, H. Y.; Purcell, E. M. *Phys. Rev.* **1954**, *94*, 630. (b) Meiboom, S.; Gill, D. *Rev. Sci. Instrum.* **1958**, *29*, 688.
(6) Garroway, A. N. *J. Magn. Reson.* **1977**, *28*, 365.
(7) Wind, R. A.; Emid, S.; Ligthelm, D. J.; Pourquié, J. F. J. M.; Smidt, J. *Bull. Magn. Reson.* **1984**, *6*, 71−88.

10.1021/ja0127133 CCC: $22.00

Chart 1

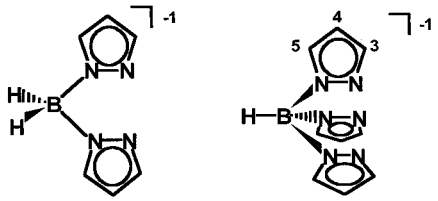

Bis(pyrazolyl)borate Tris(pyrazolyl)borate

diffusion within the whole ^{1}H spin bath. However, the requirement of methyl groups in the chemical system of interest is limiting. The purpose of this report is to describe a general approach utilizing paramagnetic dopants as a means to manage ^{1}H spin lattice relaxation times. A critical requirement of the dopant is that it must remain paramagnetic through the whole temperature range (4−100 K in this case). Further, there must be strong electron−nuclear interactions that can be spin diffused to the entire proton spin bath, which can be facilitated by methyl groups in the dopant. We have applied this methodology to the characterization of the ^{67}Zn NMR parameters of a series of four- and six-coordinate zinc complexes containing poly(pyrazolyl)-borate ligands (Chart 1) that model systems of biological interest.

The poly(pyrazolyl)borate complexes were chosen for several reasons. The most important reason is that these ligand systems allow the preparation of monomeric complexes in which the coordination geometry of ions such as Cd^{2+} and Zn^{2+} can be controlled by changing the substituents on the ligands. In many other ligand systems, when substituents are changed the whole structure changes limiting the ability to investigate the consequences of the substituent modification on the metal. The poly-(pyrazolyl)borate complexes (or their analogues) enable the possible separation of structure and property variation; for example, is the change in a particular magnetic resonance parameter due to changes in structure or due to changes in the electronic properties of the substituent? Utilizing ^{113}Cd NMR as a surrogate probe for Zn^{2+}, we[8] were able to demonstrate how sensitive ^{113}Cd shielding tensors are to changes in structure. One of the aims of the present work is to determine how sensitive the corresponding ^{67}Zn NMR parameters are to the same structural changes that were observed in previous ^{113}Cd NMR investigations.

In this report, based on the results of pulsed EPR and low-temperature proton NMR experiments, we discuss the utility of $[HB(3,4,5\text{-}Me_3pz)_3]_2Fe$ as a paramagnetic dopant for low-temperature solid-state NMR spectroscopy. Further, through a combination of low temperatures (10 K) at modest magnetic field (9.4 T), high-field (18.8 T) room-temperature solid-state ^{67}Zn NMR, and low-temperature X-ray crystallography, we examine the temperature-dependent phase transition of $[HB(3,5\text{-}Me_2pz)_3]_2Zn$. Finally, we discuss the utility of predicting the observed quadrupole coupling constants, C_q, and asymmetry parameters, η_q, for zinc using ab initio molecular orbital methods.

Table 1. Summary of Zn-Poly(pyrazolyl)borate Structural and NMR Parameters

	1[a,b]	**2**[c,d]	**3**[e]	**4**[f]
$\langle r_{ZnN}\rangle_{avg}$	2.17	2.15	2.00	2.00
$(\langle r_{ZnN}\rangle_{avg} - r_{ZnN})_{extreme}$	0.02, −0.02	0.01, −0.02	0.01, −0.00	0.01, −0.010
$\langle\theta_{NZnN}\rangle_{avg}$	90	90.0	112.4	109.8
$(\langle\theta_{NznN}\rangle_{avg} - \theta_{NZnN})_{extreme}$	3.9, −4.1	4.8, −7.0	13.2, −21.5	13.3, −12.5
θ_{BZnB}	180.0	178.4	163.2	143.0
δ_{iso} (ppm)[g]	99/92	109/199/112	158	119
C_q (MHz)	2.50/4.17	3.94/3.96/4.17	15.27	13.66
η_q	0.77/0.59	0.41/0.42/0.33	0.90	0.87
$\Delta\sigma$ (ppm)	−125/141	−132/−101/−123		
η_σ	0.13/0.22	0.86/0.67/0.54		
α (°)	69/−6	56/91/84		
β (°)	15/92	−18/−23/−18		
γ (°)	71/131	161/122/97		

[a] Looney, A.; Han, Runyu, H.; Gorrell, I. B.; Cornebise, M.; Yoon, K.; Parkin, G.; Rheingold, A. L. *Organometallics* **1995**, *14*, 274. [b] Lineshape parameters extracted from 9.4 T at 10 K/18.8 T @ room temperature (see Results and Discussion). [c] Reference 31. [d] Lineshape parameters extracted from 9.4 T at 10 K/11.7 T at 10 K/18.8 T @ room temperature (see Results and Discussion). [e] Reference 12. [f] Reger, D. L.; Wright, T. D.; Smith, M. D.; Rheingold, A. L.; Rhagitan, B. *J. Chem. Crystallogr*. **2000**, *30*, 665. [g] Isotropic chemical shifts are uncorrected for temperature and susceptibility of the cryostat.

Experimental Section

Synthesis. $[HB(3,4,5\text{-}Me_3pz)_3]_2Fe$,[9] $[HB(3,5\text{-}Me_2pz)_3]_2Zn$[10] [**1**], $[HB(pz)_3]_2Zn$[11] [**2**], $[H_2B(3,5\text{-}Me_2pz)_2]_2Zn$[12] [**3**], and $[H_2B(pz)_2]_2Zn$[13] [**4**] were prepared by published methods. The zinc samples doped (2 to 4%) with $[HB(3,4,5\text{-}Me_3pz)_3]_2Fe$ were prepared by dissolving the corresponding poly(pyrazolyl)borate zinc(II) complex with $[HB(3,4,5\text{-}Me_3pz)_3]_2Fe$ in CH_2Cl_2 (10 mL). The homogeneous solution was evaporated to leave a pink to reddish solid. The uniform distribution of the dopant is necessary to efficiently relax the whole proton spin bath (a physical mixture of the solids is not sufficient).

X-ray Studies. Colorless crystals of **1**−**4** were coated in inert oil and placed on the end of a thin glass fiber. X-ray intensity data were collected on a Bruker SMART APEX CCD-based diffractometer system using Mo Kα radiation (λ = 0.71073 Å). Crystal quality and unit cell parameters were initially determined at 298 K on the basis of reflections harvested from a set of three scans measured in orthogonal wedges of reciprocal space. These parameters matched those reported in the published structures (see Table 1). The crystals were cooled to 120 K, and the unit cell parameters were checked again. Only small changes, expected from the temperature change, were observed for **2**−**4**. Crystals of **1** exploded around 185 K, with both rapid and slow cooling regimes, leaving no solid on which to check the unit cell.

EPR Measurements. All of the EPR measurements were performed on a Bruker ESP380E pulsed EPR spectrometer operating near 9.7 GHz. The sample was measured in an MD5 dielectric resonator in an Oxford CFG-935 cryostat whose temperature was controlled by an Oxford ITC-503 temperature controller.

Samples for EPR contained 20 mM stable nitroxide radical, TEMPO, as an EPR-active reporter of the spin dynamics of metal ion dopants. The samples included the following: a blank containing TEMPO in a 1:1 mixture of $CDCl_3$:CD_3OD; 12.7 mM $[HB(3,4,5\text{-}Me_3pz)_3]_2Fe$ with

(8) (a) Reger, D. L.; Mason, S. S.; Rheingold, A. L.; Ostrander, R. L. *Inorg. Chem*. **1993**, *32*, 5216. (b) Lipton, A. S.; Mason, S. S.; Reger, D. L.; Ellis, P. D. *J. Am. Chem. Soc*. **1994**, *116*, 10182. (c) Reger, D. L.; Myers, S. M.; Mason, S. S.; Darensbourg, D. J.; Holtcamp, M. W.; Reibenspies, J. H.; Lipton, A. S.; Ellis, P. D. *J. Am. Chem. Soc*. **1995**, *117*, 10998. (d) Reger, D. L.; Myres, S. M.; Mason, S. S.; Rheingold, A. L.; Haggerty, B. S. *Inorg. Chem*. **1995**, *34*, 4996. (e) Reger, D. L.; Mason, S. S. *Organometallics* **1993**, *12*, 2600. (f) Lipton, A. S.; Mason, S. S.; Myers, S. M.; Reger, D. L.; Ellis, P. D. *Inorg. Chem*. **1996**, *35*, 7111−7117. (g) Reger, D. L.; Collins, J. E.; Myers, S. M.; Rheingold, A. L.; Liable-Sands, L. M. *Inorg. Chem*. **1996**, *35*, 4904. (h) Reger, D. L.; Collins, J. E.; Rheingold, A. L.; Liable-Sands, L. M. *Inorg. Chem*. **1999**, *38*, 3235. (i) Reger, D. L.; Collins, J. E.; Jameson, D. L.; Castellano, R. K. *Inorg. Synth*. **1998**, *32*, 63. (j) Reger, D. L. *Comments Inorg. Chem*. **1999**, *1*, 21.

(9) Trofimenko, S. *J. Am. Chem. Soc*. **1967**, *89*, 6288.
(10) Looney, A.; Han, R.; Gorrell, I. B.; Cornebise, M.; Yoon, K.; Parkin, G. *Organometallics* **1995**, *14*, 274.
(11) Trofimenko, S. *J. Am. Chem. Soc*. **1966**, *88*, 1842.
(12) Dias, H. V. R.; Gorden, J. D. *Inorg. Chem*. **1996**, *35*, 318.
(13) Jesson, J. P.; Trofimenko, S.; Eaton, D. R. *J. Am. Chem. Soc*. **1967**, *89*, 3148.

20 mM TEMPO in a 1:1 mixture of $CDCl_3$:CD_3OD; and 6.7 mM Cr(acac)$_3$ (acac = acetylacetonato) with 20 mM TEMPO in CD_3OD. About 0.2 mL of each sample solution was placed into a Wilmad 707-SQ quartz EPR tube and frozen by lowering the tube into liquid nitrogen.

A two-pulse, primary echo sequence was used to measure the decay of the electron spin echo of the TEMPO as a function of the time between the two microwave pulses at the maximum of the signal from TEMPO. The spin lattice relaxation rate of the TEMPO probe was measured by saturating its EPR signal by a train of microwave pulses followed, after a time delay, by a two-pulse echo sequence to generate an electron spin echo, which was used to monitor recovery of the TEMPO EPR signal from saturation. The time delay for recovery was increased in roughly equal logarithmic steps from 8 ns to 0.8 s. No signals were seen from either metal dopant. Measurements were made every 5 K from 10 or 15 K to 60 K.

The experimental relaxation curves were analyzed using nonlinear least-squares fits of theoretical kinetic curves to the data using Mathematica 4.1.

NMR Measurements. The solid-state ^{113}Cd NMR experiment on [H_2B(3,5-Me_2pz)$_2$]$_2$Cd was performed on a Varian Infinity spectrometer in a wide-bore Oxford magnet operating at 7.05 T (66.547 MHz Larmor frequency for ^{113}Cd). The samples were ground and packed into 7.5 mm o.d. zirconia rotors with Kel-F end caps for use in a Varian/Chemagnetics PENCIL MAS probe. All chemical shifts and tensors elements are referenced to an external sample of 0.1 M Cd(ClO_4)$_2$ in a 1:1 H_2O/D_2O solution at 25 °C, with positive shifts denoting resonances to lower shielding. The pulse sequence used was a single contact CP[4] sequence with proton decoupling. The ^{1}H $\pi/2$ was 5 μs, the contact time used was 6 ms, the recycle delay was 10 s, and the spinning speed was 3 kHz. The principal elements of the shielding tensor and the isotropic chemical shift were extracted from the experimental data determined using the program STARS[14,15] on a SUN Ultra 10 computer.

The low-temperature ^{1}H and ^{67}Zn experiments were performed using a Varian Infinity^{Plus} console with a widebore Oxford Instruments magnet operating at 9.4 T in combination with home-built components. Additional low-temperature measurements were made on a Varian Unity^{Plus} spectrometer with a widebore Oxford magnet operating at 11.7 T, data not shown. The low-temperature ^{1}H measurements were performed as a variation on the basic two-pulse $90_x - \tau - 90_{\pm y} - \tau$ solid echo experiment.[16] For example, the ^{1}H relaxation, T_1, measurements were performed as arrays of the recycle delay time for a fixed value of τ in the solid echo. Hence, the relaxation times reported here represent only "operational" estimates for T_1 used for setting up a given experiment. The $T_{1\rho}$ experiments were performed in a similar manner; that is, a spin-locking pulse was applied after the first $90_x°$ pulse followed by the remainder of the echo sequence. Typical values for 2τ and the 90° pulse width used in these experiments were 60 and 4.2 μs, respectively.

The ^{67}Zn experiments were performed at 10 K utilizing CP[4] and a train of CPMG[5] spin echoes, or the CP/QCPMG pulse sequence. The basic theory underpinning the spikelet experiment is described elsewhere.[17] Typical values for the experimental parameters used are ^{1}H $\pi/2$ pulse duration of 4.2 μs, a selective ^{67}Zn π pulse width of 4 ms, and a spectral width of 1 MHz. The details of the associated low-temperature experiments have been published elsewhere.[2] Complexes **1** and **2** were acquired with single contact CP and a recycle time of 30 s for 2048 transients. Complex **3** was acquired with two contacts and a recycle time of 10 s for 1024 transients, and **4** was acquired with two contacts, 60 s, and 512 transients. The experimental aspects associated with the determination of the ^{67}Zn lineshape fall into two discrete categories that depend on the overall width (baseline to baseline) of the lineshape. The first is when the observed width of the lineshape is less than the excitation profile associated with the CP sequence. In the experiments reported here, the excitation profile corresponds to ~50 kHz. In this case, the spectrum is recorded normally and then analyzed. This situation is found for the six-coordinate pyrazolylborates complexes reported here. However, when the width of the lineshape exceeds this nominal value, the spectrometer frequency must be arrayed using a step size that is consistent with the excitation profile. The number of steps in the array depends on the width of the spectrum. This latter procedure was necessary for the four-coordinate pyrazolylborate complexes. Because such situations are uncommon in normal CP experiments, we will outline our method for obtaining the resulting lineshape.

The first step is to gain an understanding of the excitation bandwidth of the probe. For the selective observation of the $\pm^1/_2$ transition for a quadrupolar nuclide with nuclear spin of S under conditions of CP, the excitation bandwidth can be estimated from the following equation:

$$\omega_{1S}/2\pi = \omega_{1H}/[2\pi(S + {}^1/_2)] = 1/[(S + {}^1/_2)4\tau^{H}_{90}] \qquad (1)$$

In this equation, $\pm\omega_{1S}/2\pi$ is the approximate excitation width in hertz, and τ^{H}_{90} is the ^{1}H 90° pulse width in microseconds. In our case with a 4.2 μs for the ^{1}H 90°, $\pm\omega_{1S}/2\pi$ corresponds to ~±20 kHz. This suggests that the step size for the transmitter should be 20 kHz. The whole lineshape is then divided into bins, each bin corresponding to an excitation bandwidth. The ^{67}Zn frequency is then arrayed to these frequencies and the subspectra collected. Probe tuning is checked during the series of experiments. Typically, the probe needed retuning every ~50 kHz to maintain the "nominal" Hartmann−Hahn[18] match conditions.

The resulting phase-corrected subspectra are re-referenced (by either left or right shifting the *spectrum* the number of points corresponding to the offset or equivalently performing a frequency shift in the *time domain*). The data are then combined to form a sky projection. Figure 1 depicts one such projection and a subset of subspectra that were used in its construction. The extraction of the quadrupole and shielding parameters, in these cases, was based on the resulting lineshape depicted in these projections. Because of offset effects, it is possible to introduce a scalloping of the final spectrum. These deviations from an ideal lineshape arise from a combination of probe Q and off resonance effects on the Hartmann−Hahn match condition.

The solid-state ^{67}Zn NMR experiments on the octahedral complexes were also performed at room temperature on a 18.8 T Varian Inova spectrometer with a ^{67}Zn resonance frequency of 50.046 MHz. The high-field data were collected in a similar manner as the data obtained at lower fields using a home-built cross coil double resonance probe.[19]

All ^{67}Zn chemical shifts are referenced to a 0.5 M aqueous solution of zinc acetate at room temperature. The quadrupole tensors were extracted from the lineshapes using a combination of an in-house program and the program SIMPSON.[20] In general, the Hamiltonian governing the ^{67}Zn NMR lineshape would include not only quadrupole interactions but also the consequences of anisotropic shielding as well. In the case of the octahedral complexes, it was necessary to include anisotropic shielding. This was needed for proper placement of the magic angle feature in the ^{67}Zn lineshape. The predicted shielding contributions noted at 9.4 T were checked at 18.8 T.

Ab Initio Calculations. The calculations of the electric field gradient tensors were performed using the Gaussian 98 suite of programs.[21] The geometry determined by X-ray crystallography was used for each

(14) Bildsoe, H. *Stars User's Guide. Spectrum Analysis of Rotating Solids*; Publ. No. 87-195233-00 Rev A0296, Varian Associates Inc., Palo Alto, 1996.
(15) Skibsted, J.; Nielsen, N. C.; Bildsoe, H.; Jakobsen, H. J. *J. Magn. Reson.* **1991**, *95*, 88.
(16) Solomon, I. *Phys. Rev.* **1958**, *110*, 61.
(17) Larsen, F. H.; Jakobsen, H. J.; Ellis, P. D.; Nielsen, N. C. *J. Phys. Chem.* **1997**, *101*, 8597.
(18) Hartmann, S. R.; Hahn, E. L. *Phys. Rev.* **1962**, *128*, 2042.
(19) Sears, J. A.; Lipton, A. S.; Ellis, P. D., to be submitted.
(20) Bak, M.; Rasmussen, J. T.; Nielsen, N. C. *J. Magn. Reson.* **2000**, *147*, 296.

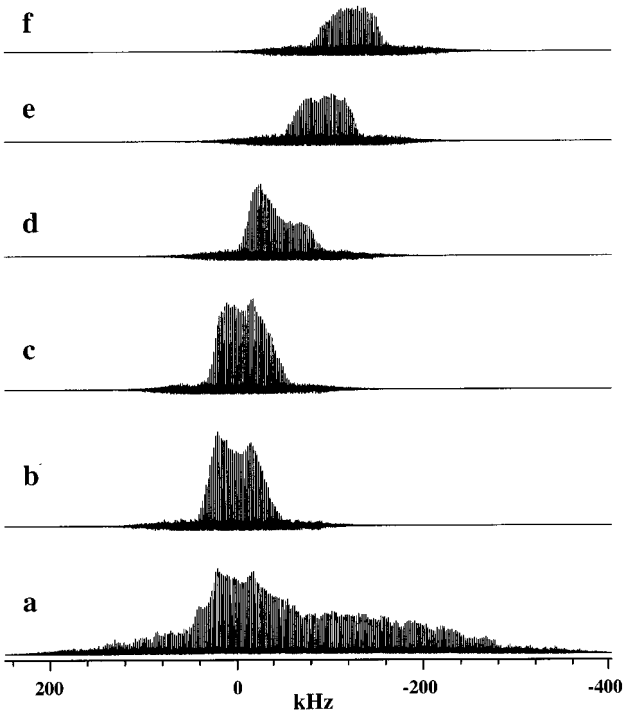

Figure 1. A sky projection (a) of ^{67}Zn solid-state NMR of $[H_2B(pz)_2]_2Zn$ obtained at 10 K and a selection of the subspectra utilized in its construction. Each spectrum is the result of 512 accumulations with two contacts and a 30 s recycle delay between transients. Data processing included 25 Hz conventional line broadening, 1500 Hz of a match filter, and zero filling to 128 K points. The total spectrum took 18 subspectra; five such subspectra are shown here with the following transmitter offsets (b) 0, (c) −20, (d) −60, (e) −100, and (f) −140 kHz.

calculation. The triple-ξ level (including polarization functions) basis set of Ahlrichs[22] was used for the calculations. The basis set for zinc was further augmented with a single p-, and d-function, and a pair f-functions using the program g98opt.[21] The coefficients derived from these calculations can be found at the end of ref 22. The density matrix used for the calculation of the field gradient calculations was computed after the scf portion of the calculation had converged to an RMS level of 10^{-8} or better. The calculations were carried out on an 8 CPU Silicon Graphics Origin 2000 computer.

Results and Discussion

Characterization of Paramagnetic Dopants. Utilization of paramagnetic dopants (such as transition metal complexes) as a means to reduce the spin lattice relaxation times of the nucleus of interest has a long and rich history in the field of NMR.[23] As a result of this history, the magnetic requirements for the dopant are clear, that is

$$T_{1e}\omega_H \approx 1 \qquad (2)$$

Here T_{1e} denotes the spin lattice relaxation time for the electron, and ω_H is the ^{1}H Larmor frequency. For ^{1}H at 9.4 T, this corresponds to a T_{1e} on the order of a few tenths of a nanosecond. The difficulty is that the T_{1e} of transition metal complexes can vary widely depending on matrix and ligands, so that some experimental determination is required.[24] The use of EPR to measure T_{1e} values of high-spin ions can be difficult because large zero-field splitting causes many of these ions to be EPR-silent and because the fields used in conventional X-band EPR are much lower than those used in modern solid-state NMR. In addition, the values of T_{1e} desired for effective nuclear relaxation are too short to measure directly by EPR, and their value must be inferred from observations of other electron or nuclear spins. In fact, as we describe below, we do not know the value of the product depicted above. That is, we could be on either side of the unity value by an order of magnitude.

Lacking specific knowledge of the aforementioned product, we must be concerned with the value of not only T_1 but also $T_{1\rho}$ for the ^{1}H's in the presence of dopants. The chemical requirements for the paramagnetic dopant are equally as clear; they must be chemically benign and soluble in the same solution as the target system. This latter requirement and our interest[8] in utilizing the novel chemistry associated with bi- and tridentate pyrazolylborate[25] type of ligands as models for the active sites of metalloproteins have dictated the use of this same ligand system for the paramagnetic dopant. In particular, we have focused our initial efforts on the high-spin $[HB(3,4,5\text{-}Me_3\text{-}pz)_3]_2Fe$ (pz = pyrazolyl ring) complex. This compound was chosen because it is chemically stable and has four unpaired electrons at all temperatures, as apposed to other [tris(pyrazolyl)-borate]$_2$Fe complexes that change to the diamagnetic, low-spin form at low temperature.[26]

Pulsed EPR. The EPR relaxation curves, either the decay of the two-pulse echo, or the recovery from saturation, are the result of a wide range of dynamic interactions in the samples. These include the following: motion of magnetic nuclei in the solvent

(21) Frisch, M. J.; Trucks, G. W.; Schlegel, H. B.; Scuseria, G. E.; Robb, M. A.; Cheeseman, J. R.; Zakrzewski, V. G.; Montgomery, J. A., Jr.; Stratmann, R. E.; Burant, J. C.; Dapprich, S.; Millam, J. M.; Daniels, A. D.; Kudin, K. N.; Strain, M. C.; Farkas, O.; Tomasi, J.; Barone, V.; Cossi, M.; Cammi, R.; Mennucci, B.; Pomelli, C.; Adamo, C.; Clifford, S.; Ochterski, J.; Petersson, G. A.; Ayala, P. Y.; Cui, Q.; Morokuma, K.; Malick, D. K.; Rabuck, A. D.; Raghavachari, K.; Foresman, J. B.; Cioslowski, J.; Ortiz, J. V.; Stefanov, B. B.; Liu, G.; Liashenko, A.; Piskorz, P.; Komaromi, I.; Gomperts, R.; Martin, R. L.; Fox, D. J.; Keith, T.; Al-Laham, M. A.; Peng, C. Y.; Nanayakkara, A.; Gonzalez, C.; Challacombe, M.; Gill, P. M. W.; Johnson, B. G.; Chen, W.; Wong, M. W.; Andres, J. L.; Head-Gordon, M.; Replogle, E. S.; Pople, J. A. *Gaussian 98*, revision A.7; Gaussian, Inc.: Pittsburgh, PA, 1998.

(22) Basis sets were obtained from the Extensible Computational Chemistry Environment Basis Set Database, Version 1/29/01, as developed and distributed by the Molecular Science Computing Facility, Environmental and Molecular Sciences Laboratory which is part of the Pacific Northwest Laboratory, P.O. Box 999, Richland, WA 99352, USA, and funded by the U.S. Department of Energy. The Pacific Northwest Laboratory is a multi-program laboratory operated by Battelle Memorial Institute for the U.S. Department of Energy under contract DE-AC06-76RLO 1830. Contact David Feller or Karen Schuchardt for further information. The augmented values of the coefficients are *p*, 0.1624500; *d*, 0.1104370; *f*, 1.443255456 and 0.158697540.

(23) (a) Blumberg, W. E. *Phys. Rev.* **1960**, *119*, 79−84. (b) Waugh, J. S.; Slichter, C. P. *Phys. Rev. B* **1998**, *37*, 4337−4339. (c) Rõõm, T. *Phys. Rev. B* **1998**, *40*, 4201−4202. (d) Waugh, J. S.; Slichter, C. P. *Phys. Rev. B* **1998**, *40*, 4203−4204.

(24) Bowman, M. K.; Kevan, L. In *Time Domain Electron Spin Resonance*; Kevan, L., Schwartz, R. N., Eds.; Wiley-Interscience: New York, 1979. Salikhov, K. M; Tsvetkov, Yu. D. In *Time Domain Electron Spin Resonance*; Kevan, L., Schwartz, R. N., Eds.; Wiley-Interscience: New York, 1979. Salikhov, K. M.; Semenov, A. G.; Tsvetkov, Yu. D. *The Electron Spin Echo and Its Applications*; Nauka: Novosibirsk, 1976. Bowman, M. K.; Norris, J. R. *J. Phys. Chem.* **1982**, *86*, 3385−3390.

(25) (a) Vahrenkamp, H. *Acc. Chem. Res.* **1999**, *32*, 589−596. (b) Weis, K.; Rombach, M.; Ruf, M.; Vahrenkamp, H. *Eur. J. Inorg. Chem.* **1998**, 263−270. (c) Looney, A.; Han, R.; McNeill, K.; Parkin, G. *J. Am. Chem. Soc.* **1993**, *115*, 4690−4697. (d) Kimblin, C.; Allen, W. E.; Parkin, G. *J. Chem. Soc., Chem. Commun.* **1995**, 1813−1815. (e) Kimblin, C.; Murphy, V. J.; Hascall, T.; Bridgewater, B. M.; Bonanno, J. B.; Parkin, G. *Inorg. Chem.* **2000**, *39*, 967−974. (f) Dowling, C.; Parkin, G. *Polyhedron* **1996**, *15*, 2463−2465. (g) Bridgewater, B. M.; Parkin, G. *J. Am. Chem. Soc.* **2000**, *122*, 7140−7141. (h) Alsfasser, R.; Trofimenko, S.; Looney, A.; Parkin, G.; Vahrenkamp, H. *Inorg. Chem.* **1991**, *30*, 4098. (i) Kimblin, C.; Hascall, T.; Parkin, G. *Inorg. Chem.* **1997**, *36*, 5680−5681. (j) Kimblin, C.; Bridgewater, B. M.; Churchill, D. G.; Hascall, T.; Parkin, G. *Inorg. Chem.* **2000**, *39*, 4240−4243.

(26) (a) Jesson, J. P.; Weiher, J. F.; Trofimenko, S. *J. Chem. Phys.* **1968**, *48*, 2058. (b) Long, G. J.; Hutchinson, B. B. *Inorg. Chem.* **1987**, *26*, 608.

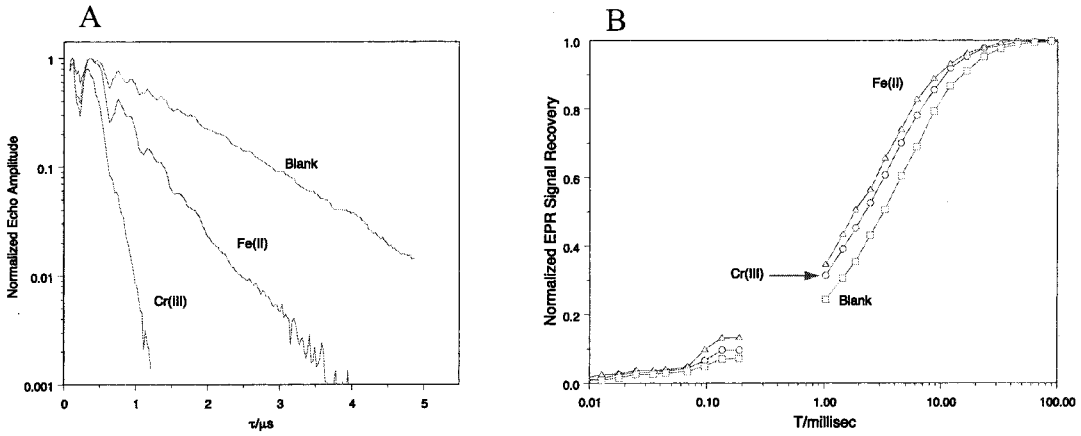

Figure 2. (a) The decay of the two-pulse electron spin echo from TEMPO as a function of the time, τ, between the two microwave pulses. (b) The recovery of the EPR signal from TEMPO as a function of time, T, following a series of eight saturating pulses. Measurements were made at 15 K at the maximum of the TEMPO EPR signal. Samples contained 2 mM TEMPO with no added dopants (blank); $[HB(3,4,5\text{-}Me_3pz)_3]_2Fe$ (Fe(II)); or $Cr(acac)_3$ (Cr(III)).

caused by lattice phonons or methyl group rotations, nuclear spin diffusion, particularly by protons, internal motion of the TEMPO probe molecule, and the dynamics of the metal dopants added to the samples. Comparing the relaxation to that of a blank that contains no metal dopant can separate the effects of the metal dopants. Figure 2 shows the decay of the two-pulse electron spin echo from TEMPO, the spin lattice relaxation of TEMPO at 15 K in the blank and samples containing the metal dopants $[HB(3,4,5\text{-}Me_3pz)_3]_2Fe$, and, for comparison, the well-known relaxation agent $Cr(acac)_3$.[27]

The two-pulse echo decay is faster with either dopant, but $Cr(acac)_3$ is particularly effective in relaxing the two-pulse echo. The echo decays show a periodic modulation in their intensity that arises from weak dipolar interactions with the deuterons within ~1 nm of the TEMPO. This modulation is predominantly at the deuterium NMR frequency of ~2.1 MHz at the 0.34 T applied field. To remove most of the modulation from the decays and to recover, as nearly as possible, the contribution to the echo decay caused by the dopant, the ratio of the echo decays with dopant to the blank was calculated. The echo decay kinetics of the blank were close to exponential at all temperatures between 15 and 60 K. The echo decay, over the full temperature range, in the Fe(II)-doped sample is described well by $\exp(-k[2\tau/\tau_c]^{1/2})$ as expected for a radical in a sample with a second paramagnetic species with rapid spin relaxation having a characteristic time constant τ_c. The kinetics of the echo decay in the $Cr(acac)_3$-doped sample were more complex. At high temperatures, the kinetic shape was similar to the Fe(II)-doped sample. As the temperature was reduced, the kinetics approached the form $\exp(-k[\tau/T_M]^{\sim 2})$. Such a functional form is expected when the T_1 of the dopant becomes comparable to or longer than the values of τ in the echo measurement. Both the kinetic form and the rate of echo decay then become highly dependent on the detailed spin dynamics of the dopant and have not been well characterized experimentally. At the lower temperatures, $T_{1Cr} \ll 1$ ms.

The overall recovery of the TEMPO from saturation is less dramatically affected by either dopant than is the phase memory decay. The gap in the data for delays between 0.2 and 1 ms is a hardware limitation of the older Bruker spectrometers. However, the recoveries with metal dopants are noticeably nonexponential. The recoveries are fit very well by an exponential recovery with a time constant T_1 and a recovery characteristic of cross relaxation to a fast relaxing species with kinetics of the form $\exp(-k[\tau/T_{CR}]^{1/2})$, where T_{CR} is a characteristic cross relaxation time. We verified that the cross relaxation component became faster and more significant at higher dopant levels.

To understand the spin dynamics responsible for the relaxation behavior observed, we examined the temperature dependence of the dopant-induced cross relaxation rate $1/T_{CR}$ in the doped samples as shown in Figure 3. For the Fe(II)-doped samples, $1/T_{CR}$ increases smoothly with increasing temperature. This indicates that the dynamic interactions responsible for cross relaxation are in the "slow motional" limit even at 60 K. The Cr(III)-doped sample, on the other hand, shows a strong peak in the cross relaxation rate at 25 K. This peak occurs when the spectral density function for one of the interactions in the dipolar interaction between TEMPO and $Cr(acac)_3$ is maximum. The "B" term involving S^+I^- and S^-I^+ operators in the dipolar Hamiltonian is likely to be responsible for this behavior.[28] In which case, $T_{CR} \propto T_{2Cr}/(1 + T_{2Cr}^2\Delta\omega^2)$, where T_{2Cr} is the spin−spin relaxation time of the $Cr(acac)_3$, and $\Delta\omega$ is the difference in EPR frequencies of TEMPO and Cr(III)$acac_3$. If we consider only the $+^1/_2$ to $-^1/_2$ transition of the $S = {}^3/_2$ Cr(III), the frequency difference will be determined by the overlap of the center of the TEMPO spectrum and the $+^1/_2$ to $-^1/_2$ transition of the Cr(III). The energy corresponding to this frequency difference will be taken up by dipolar interactions among the electron spins or by flips of the nitrogen or protons in the TEMPO. Consequently, $1/T_{2Cr}$ will correspond to a few tens or hundreds of megahertz, consistent with an echo from the Cr(III) not being observed. On the other hand, the TEMPO T_M was strongly reduced by the Cr(III), indicating that below 25 K, $1/T_{1e} < 1$ MHz, so that $T_{1e} \gg T_{2e}$.

The echo decays in the Fe(II)-doped sample are straightforward to analyze. Kinetics of the form $\exp(-k[2\tau/\tau_c]^{1/2})$ observed over the entire temperature range are expected when the dipolar fields from rapidly relaxing spins cause dephasing of the electron

(27) Gansow, O. A.; Burke, A. R.; LaMar, G. N. *Chem. Commun.* **1972**, 456.

(28) Slichter, C. P. *Principles of Magnetic Resonance*, 3rd ed.; Springer-Verlag: New York, 1996; Chapter 3.

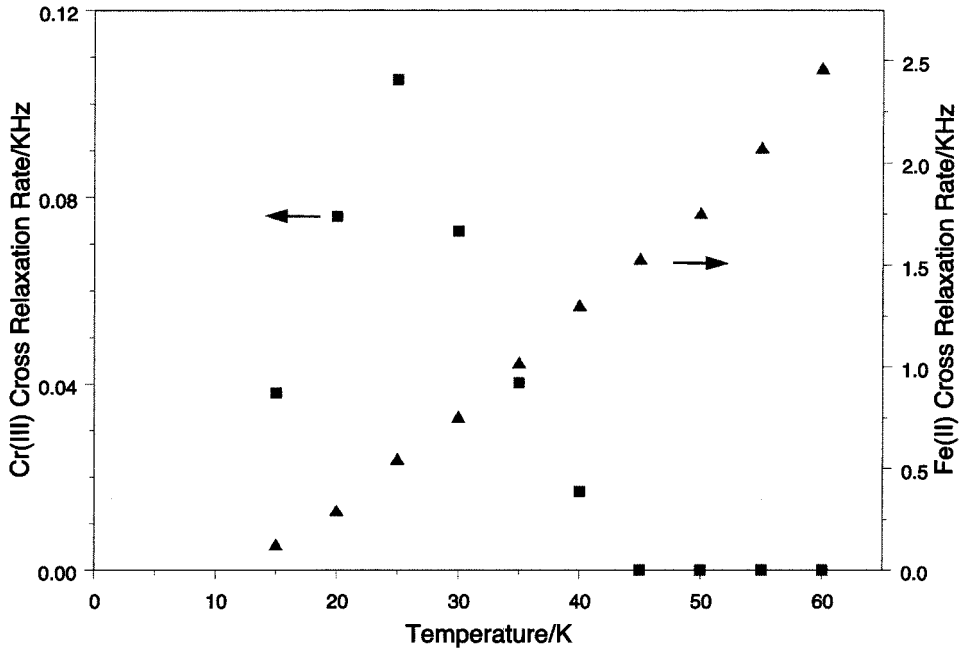

Figure 3. Measured cross relaxation rates as a function of temperature from TEMPO to $[HB(3,4,5\text{-}Me_3pz)_3]_2Fe$ (◆) or $Cr(acac)_3$ (■) determined from fits to the recovery of the TEMPO EPR signal from saturation.

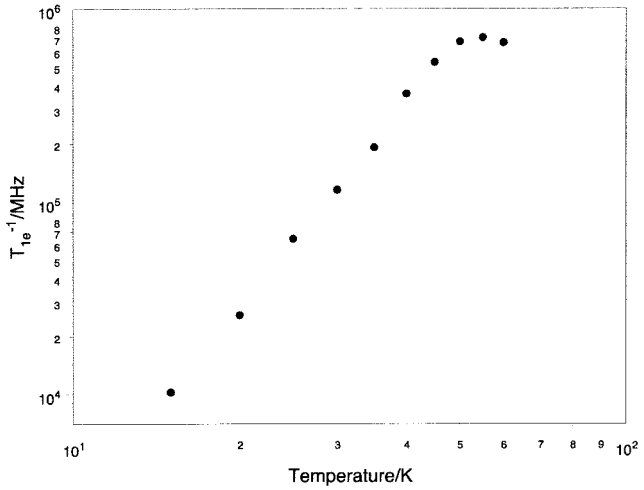

Figure 4. Temperature dependence of the correlation time ($T_{1e} = T_{2e}$) for the $[HB(3,4,5\text{-}Me_3pz)_3]_2Fe$ spin as estimated from the decay of the TEMPO electron spin echo.

spin echo. The parameter "*k*" is given as $16\pi^{3/2}/27[S_{Fe}(S_{Fe} + 1)]^{1/2}\gamma_{TEMPO}\gamma_{Fe}h/(2\pi)C_{Fe}$, where C_{Fe} is the concentration of Fe(II). This formula ignores the presumably large zero-field splitting of the Fe(II) and any orientation dependence of the correlation time for the Fe(II) spin, and so must be regarded more as an indication of the order of magnitude of relative relaxation dynamics than as a numerically accurate method to determine τ_c. With that caution in mind, the correlation time for the Fe(II) spin was calculated from the fits to the echo decays and the concentration of Fe(II) assuming that $g_{Fe} \approx 2$. The result is shown in Figure 4. The numerical values for $1/\tau_c$ are quite large, but they are in the range of $\omega_{EPR} \approx 6 \times 10^4$ MHz for TEMPO at these fields, and are assumed to correspond to $1/T_{1e}$ for the Fe(II). The temperature dependence of $1/T_{1e}$ is proportional to the fourth power of the temperature (T^4), which is close to the T^5 expected from the Orbach−Blume relaxation for a spin multiplet.[29] Finding a rapid relaxation for the Fe(II) suggests that the cross relaxation caused by the Fe(II) discussed above results from the so-called "C" and "D" terms in the dipolar Hamiltonian and that $T_{1Fe}\omega_{TEMPO} > 1$ below 50 K.[28]

Thus, we have been able to estimate the magnitudes and temperature dependences of relaxation for both dopants from the EPR measurements on a TEMPO probe radical. These estimates are obtained at a magnetic field of ∼0.34 T. The magnetic field dependence has not been extensively investigated at the fields typically used in NMR. The greater availability of high-field pulsed EPR would significantly improve the ability to predict the effect of these dopants. Theoretical treatments of the Raman relaxation process for transition metal ions predict relaxations that scale as the square of the field or B^2 for ions whose spin, *S*, is an integer and B^4 for ions with spins that are "half-integral".

For the case of the Fe(II) dopant, it would appear that ($T_{1e}2\pi$ 9.7 GHz) > 1 below at least 50 K. Thus, going up to an ∼28-fold higher field for a 400 MHz ^{1}H frequency, the T_{1e} would decrease by a factor of 28^2 or 784, while the relevant frequency would be that of a ^{1}H (400 MHz) rather than that of the TEMPO (9.7 GHz). Thus, the product would decrease by 19 012 and likely become much less than unity at 50 K. The temperature dependence of $1/T_{1e}$ is proportional to the temperature raised between the fourth or fifth power ($T^{4,5}$) and should bring the product to a value near unity at 5−10 K, making the Fe(II) an effective dopant.

The data indicated that T_{1e} for the Cr(III) was much greater than 1 ms at low temperatures. At the field corresponding to ^{1}H at 400 MHz, the T_{1e} should decrease by 28^4 ($\sim 6 \times 10^5$) and, if it depends as T^5, increase 5^5 (or 3125) as the temperature is dropped from 25 to 5 K. The result is a T_{1e} on the order of 1/200 μs, giving $T_{1e}\omega_{NMR} \approx 13$, making Cr(III) a poor relaxant for the ^{1}H T_1 at low temperature, but potentially a significant relaxant for the ^{1}H $T_{1\rho}$.

(29) Blume, M.; Orbach, R. *Phys. Rev.* **1961**, *127*, 1587.

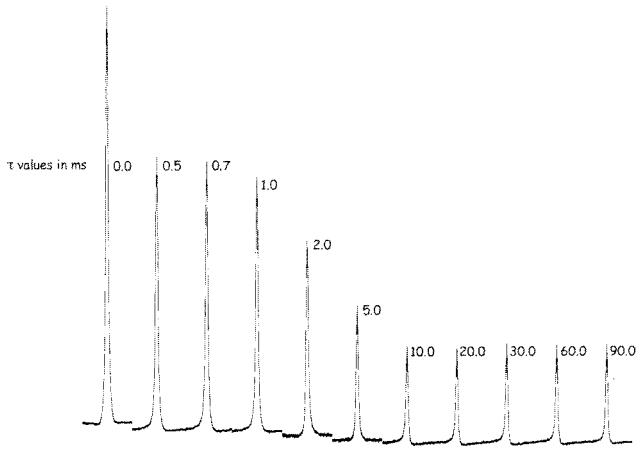

Figure 5. Representative ^{1}H $T_{1\rho}$ experiment performed at 10 K. The τ values are indicated for each experiment. The acquisition details are described in the text.

Solid-State ^{1}H NMR. Crucial to the success of the low-temperature experiments reported below is the utilization of the cross polarization (CP) experiment as a means to generate the ^{67}Zn magnetization. As stated above, we have utilized paramagnetic dopants as a means to manage the ^{1}H relaxation times T_1 and $T_{1\rho}$. To guide us in the selection of these dopants, we have utilized pulsed EPR measurements to try to estimate the product of $T_{1e}\omega_H$ for each dopant. The measurements suggest that dopants containing Fe^{2+} will meet *all* of the relaxation criteria mentioned above. An example of a successful $T_{1\rho}$ experiment on **1** using 2% $[HB(3,4,5\text{-}Me_3pz)_3]_2Fe$(II) at 10 K is depicted in Figure 5. This figure is representative of all of the successful $T_{1\rho}$ experiments. The data are not easily fit by a single value of $T_{1\rho}$. However, these data can be analyzed in terms of two time constants: a fast $T_{1\rho}$ process on the order of 1 ms and a slow $T_{1\rho}$ process >100 ms. The fast process (accounting for ~65% of the magnetization) presumably represents the fraction of the protons undergoing rapid spin diffusion to the electron relaxation sink. The slow process represents that fraction (accounting for the remaining ~35% of the magnetization) of the protons which is remote to the electron. It is this latter fraction of protons which provides the ^{67}Zn magnetization. However, $Cr(acac)_3$ represents an example of a dopant that will *not* meet these requirements. The latter provided the needed reduction in T_1 but shortens the values of T_2 and $T_{1\rho}$ to such an extent that the CP experiment can no longer be performed. In the analogous $T_{1\rho}$ experiment for the $Cr(acac)_3$-doped sample, two negative observations were noted; the proton magnetization was reduced to about 10% of the available magnetization at 30 ms as compared to 25% for the Fe(II) dopant, and the total signal-to-noise ratio in the proton spectrum was reduced by at least an order of magnitude.

Solid-State ^{67}Zn NMR. The use of a dopant has enabled the low-temperature ^{67}Zn solid-state NMR experiments reported here. We illustrate the utility of this approach by characterization of four- and six-coordinate zinc poly(pyrazolyl)borate complexes. As an aid in the understanding of the structural consequences on the ^{67}Zn NMR parameters, we have included in Figure 6 the structure of compounds **1**−**4**. Figure 6a and b denotes **1** and **2**, respectively, whereas, Figure 6c and d denotes **3** and **4**, respectively. The NMR parameters extracted from these data are listed in Table 1 along with a summary of pertinent structural data for each complex. In summarizing the structural data in the Tables and the following discussion, we have assumed an uncertainty in the bond distances and angles of ±0.005 Å and ±0.2°, respectively. Inclusion of anisotropic shielding introduces five more parameters ($\Delta\sigma$ and η_σ and three Euler angles that relate the shielding and quadrupole frames) to the fitting procedure. Naturally, the rms error would be reduced by such a procedure, and the overall fit to the experimental spectra is improved. The value of $\Delta\sigma$ is reported with the following conventions:

$$\Delta\sigma = \delta_{33} - {}^1/_2(\delta_{11} + \delta_{22}), \quad \eta_\sigma = (\delta_{22} - \delta_{11})/(\delta_{33} - \delta_{iso}) \tag{3}$$

where

$$|\delta_{33} - \delta_{iso}| \geq |\delta_{11} - \delta_{iso}| \geq |\delta_{22} - \delta_{iso}| \tag{4}$$

and

$$\delta_{iso} = (\delta_{11} + \delta_{22} + \delta_{33})/3 \tag{5}$$

Octahedral Complexes. The low-temperature solid-state ^{67}Zn NMR spectra of the octahedral complexes **1** (Figure 6a) and **2** (Figure 6b), doped with ~2% of $[HB(3,4,5\text{-}Me_3pz)_3]_2Fe$, obtained at 9.4 T are depicted in Figure 7 along with their respective simulations. The values for C_q and η_q extracted from these spectra are 2.53 MHz and 0.58; 3.94 MHz and 0.41, respectively. These fits both include contributions from chemical shielding. The placement of the magic angle features and experiments performed at 11.7 T (data not shown) indicated that this inclusion was necessary to describe each of the spin systems.

The width of the lineshape at 9.4 T for both octahedral complexes is such that we could perform a room-temperature experiment at 18.8 T. These data aid in the extraction of the contribution to the overall lineshape that may arise from anisotropic shielding (which increases with field, while the second-order quadrupolar contribution decreases). The room-temperature data for complex **2** were consistent with the values of C_q and η_q extracted from the 10 K, 9.4 T lineshape; however, the best fit of all seven parameters resulted in slightly different parameters. The values extracted from the room-temperature, high-field data were a C_q of 4.1 MHz and an η_q of 0.32. The differences may be due to changes in the crystal packing between the different temperatures. The high-field spectrum is contrasted with its optimized simulation, and the predicted low-field spectrum (generated from these parameters) is compared to its respective experimental data in Figure 8.

Conversely for complex **1**, there is significant disagreement between the values of C_q and η_q obtained from the two different temperatures and fields. Further, the sign of the shielding anisotropy is inverted between the two experimental conditions. The data obtained at 18.8 T and room temperature with its corresponding simulation are depicted in Figure 9. The values of C_q and η_q extracted from the room-temperature spectrum of **1** are 4.47 MHz and 0.33. The difference between the low-field, low-temperature (C_q of 2.53 MHz) and high-field ambient-temperature (C_q of 4.47 MHz) data can be explained if **1** undergoes a temperature-dependent phase transition. Attempts to determine the structure of the low-temperature phase failed

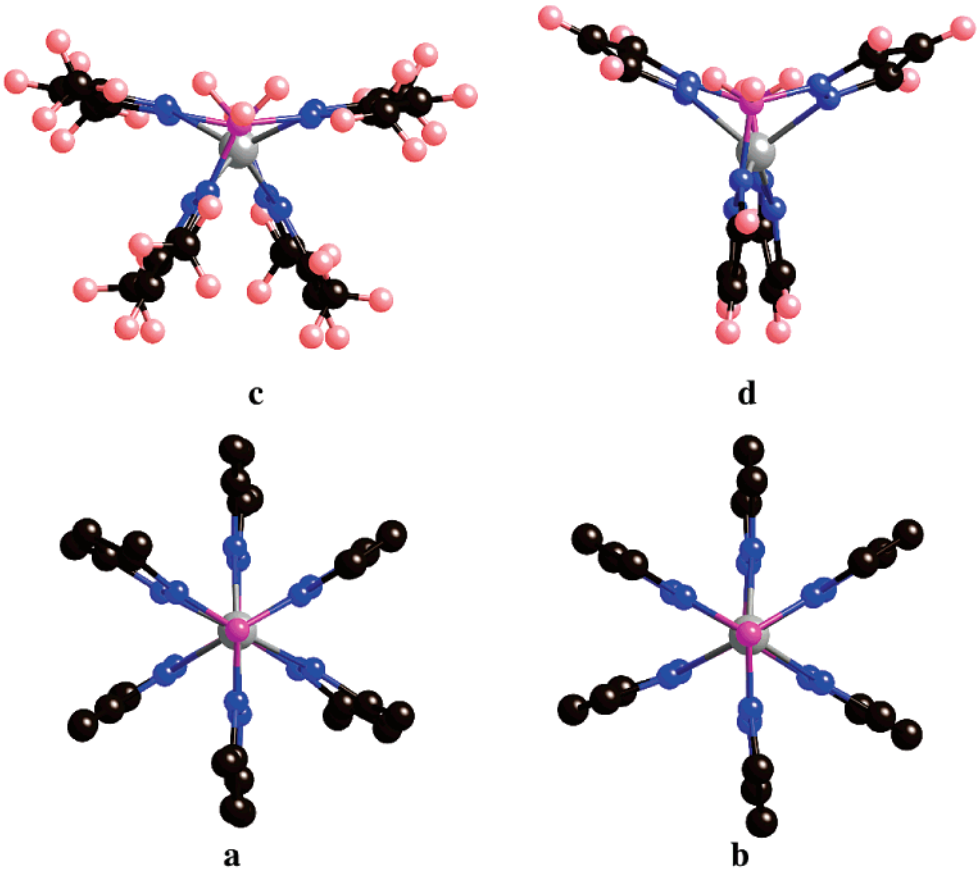

Figure 6. Structures **1**−**4** are depicted. The octahedral complexes **1** and **2** are shown as (a) and (b), respectively. Likewise, the tetrahedral complexes **3** and **4** are denoted as (c) and (d), respectively. Each structure is depicted in an orientation such that the vector connecting HB···BH fragments of the pyrazolylborate ligand is normal to the page.

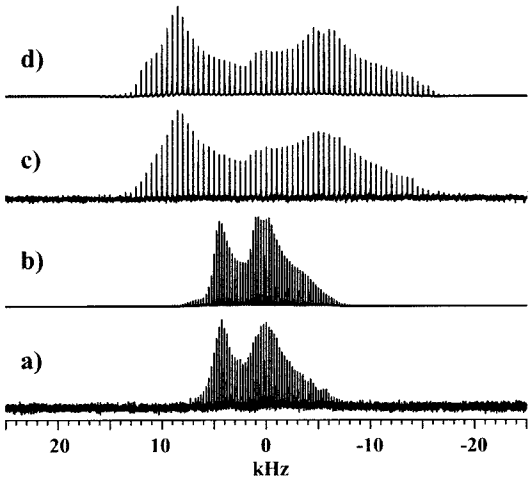

Figure 7. Low-temperature spectra (a and c) and simulations (b and d) of $[HB(3,5\text{-}Me_2pz)_3]_2Zn$ and $[HB(pz)_3]_2Zn$, respectively. Data were acquired at 9.4 T and 10 K with 250 Hz spike separations, 1568 transients, recycle time of 30s and 500 Hz spike separations, 1174 transients, recycle time of 60 s for **1** and **2**, respectively. Each experiment utilized a 30 ms contact time and 25 echoes in the train. Simulations utilize parameters listed in Table 1.

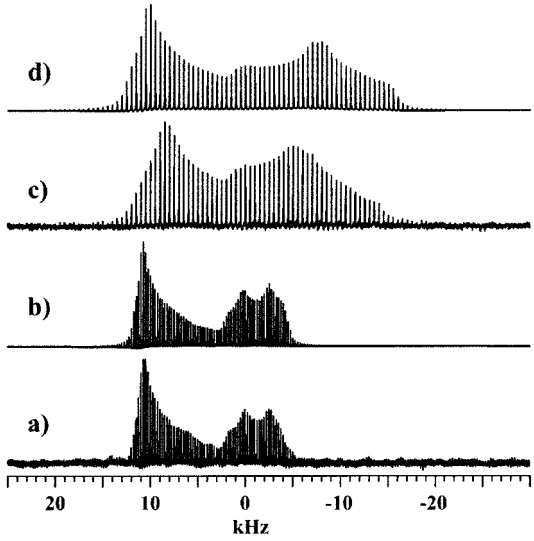

Figure 8. Experimental (a and c) and simulated (b and d) data $[HB(pz)_3]_2Zn$ acquired at 18.8 and 9.4 T, respectively. High-field data were acquired at room temperature with a recycle time of 5 s, 15 192 transients, a 25 ms contact time, and 500 Hz spike separations. The FID was zero filled between the echoes to 250 Hz spikes in the frequency domain.[2] Simulation parameters are listed in Table 1. The simulation in (d) was calculated using the parameters from (b).

dramatically when the single crystal repeatedly "exploded" at temperatures near 185 K, clearly indicating that a phase change is occurring at this temperature. However, in analogous X-ray experiments performed on complexes **2**−**4**, no phase change was observed. In addition, efforts to obtain the temperature dependence of the ^{67}Zn lineshape for **1** were frustrated by significant hysteresis.[30] As a result, we report only the lineshape at the two temperature extremes.

The quadrupole coupling constant, C_q, is a reflection of a combination of structure and electronic effects, in this case, the

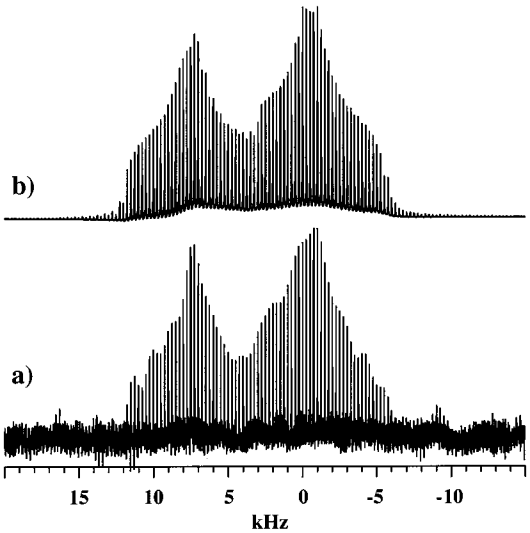

Figure 9. Experimental (a) and simulated (b) spectra of $[HB(3,5\text{-}Me_2pz)_3]_2Zn$ acquired at 18.8 T and room temperature with 32 768 transients, a recycle time of 5 s, a 25 ms contact time, and 500 Hz spike separations. The FID was zero filled between the echoes to 250 Hz spikes in the frequency domain.[2] Simulation parameters are listed in Table 1.

consequences of the addition of the methyl groups in the pyrazolyl rings. The data summarized in Table 1 clearly point to the fact that the octahedral zinc pyrazolylborate complexes are similar but *not* isostructural. In going from **2** to **1**, there is a lengthening of the average Zn−N bond distance, for example, from 2.15 to 2.17 Å. Likewise, the Zn−N bond distances in both complexes are not equal. For example, in **2** (using the labeling scheme of Nakata et al.[31] − N_{11} opposite N_{61}, N_{21} opposite N_{51}, and N_{31} opposite N_{41}), the Zn−N_{51} bond is 0.02 Å longer than the average, while the corresponding Zn−N_{41} is shorter than the average by 0.01 Å. Concomitantly, there is a difference in contiguous bond angles. In the same molecule, the N_{61}−Zn−N_{41} angle is 4.8° greater than the average, while the N_{41}−Zn−N_{21} angle is 7.0° less than the average. Similar distortions exist for **1**. Hence, the origin of the observed trend in C_q cannot simply be stated in terms of methyl substituent effects or steric interactions. Rather, the trend in C_q reflects the relative distortions that exist within the molecular framework. Further, the structure of **1** in the low-temperature phase must be such as to *reduce* the distortions around the Zn^{2+} ion or reduce by happenstance the value of the field gradient at the Zn^{2+} ion.

Tetrahedral Complexes. The sky projections denoting the ^{67}Zn NMR spectra of **3** (Figure 6c) and **4** (Figure 6d) doped with ∼2% of $[HB(3,4,5\text{-}Me_3pz)_3]_2Fe$ are shown in Figure 10 along with their corresponding simulations. Second-order quadrupole effects dominate these simulations. Further, we utilized ideal pulses in the simulation of their respective lineshapes.

The values of C_q and η_q extracted from these spectra are 15.35 MHz and 0.9, and 13.71 MHz and 0.89, respectively. The tetrahedral complexes are more distorted from ideal values than are the octahedral complexes. This increased distortion is most notably reflected in the deviation of the angles from their ideal tetrahedral values of 109.47° for the coordination angles and the B···Zn···B angle. In the absence of any distortions, this latter angle should be 180°. The measured B···Zn···B angles are

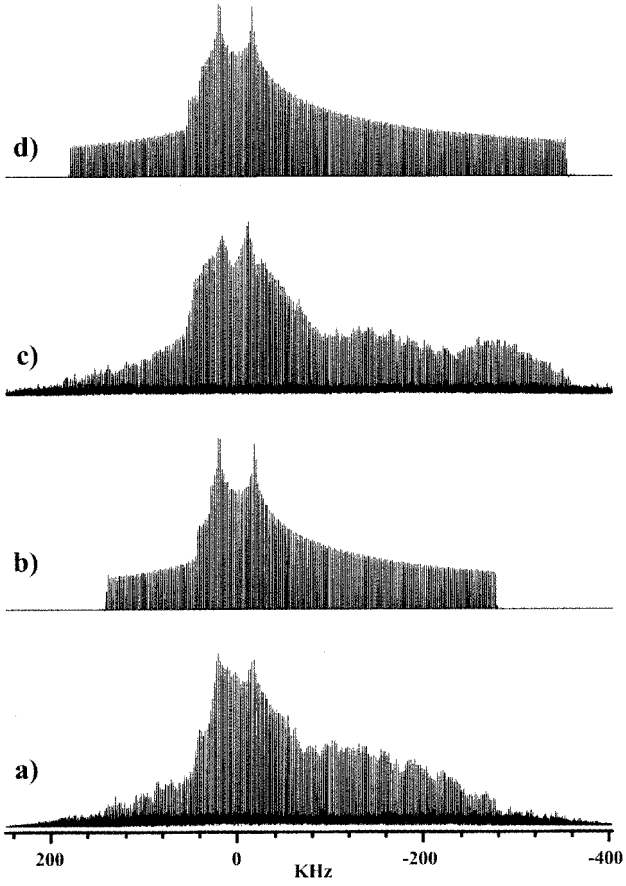

Figure 10. Sky projections for (a) $[H_2B(pz)_2]_2Zn$ and (c) $[H_2B(3,5\text{-}Me_2pz)_2]_2Zn$ and their respective simulations (b) and (d) using parameters listed in Table 1.

163.2° and 143.0° for the **3** and **4**, respectively, indicting that on the basis of this parameter **4** is more distorted. In **3**, the maximum deviation from ideal coordination angles is 21.5°, whereas in **4**, the maximum deviation is 13.3°. Hence, from the perspective of the coordination angles, **3** is the more distorted. Clearly, no one parameter is going to be a definitive measure of distortion. However, this increased distortion of the tetrahedral complexes is similarly reflected in their C_q values relative to those of the octahedral complexes, that is, C_q values on the order of 13 to 15 MHz as compared to values of 5 MHz or less for the octahedral complexes. The variation in the bond distances is less in the tetrahedral complexes than in the corresponding octahedral complexes, with **4** giving rise to the largest variation in Zn−N distances, that is, 0.01 and −0.01 Å. As in the case with the octahedral complexes, there is a concomitant distortion of the N−Zn−N angles of −12.5° and +13.3°.

In summary, the quadrupole couplings for the tetrahedral complexes increase by 12% in going from **4** to **3**. The corresponding change in the octahedral complexes going from **1** (at room temperature) to **2** is 11%.

Solid-State ^{113}Cd NMR. To facilitate the comparison between cadmium and zinc complexes, we have determined the chemical shift anisotropy of the remaining cadmium analogue, $[H_2B(3,5\text{-}Me_2pz)_2]_2Cd$ [**7**]. The chemical shift information for **7** and the other cadmium analogues is listed in Table 2 along with some structural information.

From the previous work on $[HB(3,5\text{-}Me_2pz)_3]_2Cd$ [**5**], we know the most shielded tensor element is aligned nearly ortho-

(30) Unpublished observations.
(31) Nakata, K.; Kawabata, K.; Icikawa, I. *Acta Crystallogr.* **1995**, *C51*, 1092.

Table 2. Summary of Cd-Poly(pyrazolyl)borate Structural and NMR Parameters

	5[a]	**6**[b]	**7**[c]	**8**[d]
$\langle r_{CdN}\rangle_{avg}$	2.35	2.33/2.34 0.04, −0.03	2.22	2.22
$(\langle r_{Cd}\rangle_{avg} - r_{CdN})_{extreme}$	0	0.05, −0.03	0.020, −0.02	0.03, −0.03
$\langle \theta_{NCdN}\rangle_{avg}$	90	92.7/89.8 13.8, −11.9	114.8	109.3
$(\langle \theta_{NCdN}\rangle_{avg} - \theta_{NCdN})_{extreme}$	7.3, −7.3	11.7, −12.2	22.6, −27.9	17.2, −22.1
θ_{BCdB}	180	178.0/180	142.7	154.0
δ_{iso}	175.2	207.6/177.9	335.5	291.9
$\Delta\sigma$	−210.2	−238.7/−228.4	−248.2	−280.0
η_σ	0.07	0.55/0.65	0.68	0.04

[a] Reference 8a. [b] Reference 8c. [c] Reger, D. L.; Wright, T. D.; Rheingold, A. L.; Rhagitan, B. J. *J. Chem. Crystallogr.* **2001**, *30*, 745. [d] Reger, D. L.; Mason, S. S.; Rheingold, A. L. *Inorg. Chim. Acta* **1995**, *240*, 669.

gonal to the plane of nitrogens made by the tridentate ligand. These arguments could be made due to the symmetry of **5**. It was also determined that the most deshielded element was dependent upon the tilt of the ligands. Here tilt refers to the angle made by the plane of the nitrogens within one ligand. The tilt of the plane arises from the asymmetry of the Cd−N bond lengths. Because of the size of the cadmium, these compounds are more distorted from an ideal octahedral geometry than are the analogous zinc complexes. This distortion is reflected in the larger N−Cd−N′ angles, where the intraligand angles for the cadmium complexes are typically smaller than the corresponding angles in the zinc complexes. For the cadmium, this difference is reflected in a larger contribution to the most deshielded element (and, therefore, increased chemical shift).

A direct comparison of zinc and cadmium in the octahedral complexes is not straightforward, due to differences in symmetry. In complex **5**, all Cd−N distances are equivalent, resulting in a 3-fold symmetry axis. However, in the analogous zinc system (absent the 3-fold symmetry axis), the zinc complex has one short and two long bonds per ligand, and the short bond is trans with the short bond from the other ligand. In the parent complexes, there is a short Cd−N bond that is trans between the ligands, and for the corresponding zinc system there is a long bond that is cis between the ligands. We do not have solid-state NMR data on a cadmium complex that mimics this structural feature.

In the case of the tetrahedral molecules, the parent cadmium complex [**8**] has an η_σ of 0.04. This is due to the ligand geometry despite the absence of an axis of symmetry. The N−Cd−N plane for each ligand makes an angle of 90° with the same plane of the opposing ligand. However, in the case of complex **7**, substitution of the hydrogens at the positions 3 and 5 with methyl groups introduces a steric interaction which changes the angle between the planes from 90° to 122° resulting in an increase in η_σ from 0.04 to 0.68. A further difference is reflected in the bond distances. While the average distance is practically the same for each, the parent complex has two bonds that are longer than any bond in **7**. These longer bonds give rise to the higher shielding in the parent cadmium complex.

Comparing tetrahedral cadmium structures with their zinc analogues, we see that the ligand framework is similar for each metal. That is, the average bond distance is within 0.005 Å, and the plane defined by the coordinating nitrogens and the respective metal forms similar angles. Further, each ligand has one long and one short bond in its coordination to the metal.

Table 3. Summary of Computed Quadrupole Parameters for Selected Zinc Poly(pyrazolyl)borate Complexes[a]

	1	**2**	**3**	**4**
rhf[b]				
Z_{Zn}	0.966805	0.801393	0.339097	0.427906
q_{xx}	−0.140067	−0.040450	−0.419107	0.391650
q_{yy}	−0.015987	−0.024775	−0.044568	0.063286
q_{zz}	0.156054	0.065225	0.463675	−0.454936
C_q (MHz)	5.50	2.30	16.34	16.03
η_q	0.80	0.24	0.81	0.72
dft[b]				
Z_{Zn}	0.495845	0.247252	−0.051679	0.026035
q_{xx}	−0.106117	−0.038906	−0.337206	0.314966
q_{yy}	−0.023435	−0.019670	−0.000215	0.053811
q_{zz}	0.129552	0.058576	0.337422	−0.368777
C_q (MHz)	4.57	2.06	11.89	13.00
η_q	0.64	0.33	1.00	0.71

[a] The geometries used for these calculations were the X-ray structures cited in the references for Table 1. [b] Z_{Zn} denotes the total Mulliken charge density.

Ab Initio Calculations. The poly(pyrazolyl)borate complexes investigated are small enough to perform ab initio molecular orbital calculations of the field gradient tensor. The calculations were performed with the restricted Hartree−Fock (rhf) and density functional theory (dft) methods. The poly(pyrazolyl)-borate complexes studied here have the advantage of being electrically neutral. Further, they lack the complications of hydrogen-bonding interactions. Hence, the calculations should reflect the ability of these computational methods, coupled with their basis sets, to predict zinc magnetic resonance parameters. The quadrupole coupling constant C_q is given by

$$C_q = q_{zz}[e^2/(a_0{}^3h)]Q \tag{6}$$

Here Q is the quadrupole moment of the nucleus in question, and q_{zz} is the zz element of the field gradient tensor. The atomic constants (e, a_0, and h) have their usual meanings. The zz element of the field gradient tensor, q_{zz}, and its corresponding asymmetry parameter, η_q, are defined[32] as

$$|q_{zz}| \geq |q_{xx}| \geq |q_{yy}| \tag{7}$$

and

$$\eta_q = (q_{yy} - q_{xx})/q_{zz} \tag{8}$$

In the case of ^{67}Zn, using the value of Q for ^{67}Zn (0.15×10^{-24} cm^2) summarized in Harris and Mann,[33] eq 6 can be rewritten as

$$C_q = q_{zz} \bullet 35.24473 \text{ MHz} \tag{9}$$

The results of these calculations are summarized in Table 3. Both methods are qualitatively in agreement with experiment. The quadrupole coupling constants should be larger for the tetrahedral complexes than for the octahedral complexes. Further, both methods order correctly the trends within the octahedral complexes. For example, in the octahedral complexes,

(32) Spiess, H. W. Rotation of Molecules and Nuclear Spin Relaxation. In *NMR Basic Priciples and Progress*; Dielhl, P., Fluck, E., Kosfeld, R., Eds; Springer: New York, 1978; Vol. 15, pp 55−214.
(33) Harris, R. K. Introduction. In *NMR and the Periodic Table*; Harris, R. K., Mann, B. E., Eds.; Academic Press: New York, 1978; pp 1−19.

the experimental value of C_q in **1** is larger (4.47 MHz, room temperature, 18.8 T) than the C_q in **2** (3.94 MHz). From the values summarized in Table 3, the predicted values for C_q by the dft method (4.57 MHz as compared to 2.06 MHz) and by the rhf method (5.5 MHz as compared to 2.3 MHz) are in reasonable agreement with experiment. It is interesting to note that both methods predict the values for C_q in close agreement with the experimental values obtained at room temperature. However, the ability of theory to predict the trends within the tetrahedral complexes is mixed. Experimentally, the value for C_q in **3** is 15.4 MHz, while the value for **4** is 13.7 MHz. In contrast to the octahedral case, the rhf method predicts 16.34 MHz for **3** and 16.03 MHz for **4** (the correct order), while the dft methods predict the reverse order 11.89 MHz for **3**, and 13.0 MHz for **4**.

Summary and Conclusions

The use of paramagnetic reagents with the appropriate T_{1e} relaxation characteristics has a profound enabling effect on low-temperature solid-state CP NMR experiments. The CP experiment has the demanding prerequisites that not only must the ^{1}H T_1 be reduced by the presence of the paramagnetic complex, but the $T_{1\rho}$ of the ^{1}H's must be minimally affected as well. In the absence of dopants, the NMR results for complexes **2** and **4** could not be obtained. The present investigation has utilized iron(II) coordinated to tris(pyrazolyl)borate ligands, $[HB(3,4,5\text{-}Me_3pz)_3]_2Fe(II)$, as the relaxation agent. However, other metal centers (unpublished results), including tris(pyrazolyl)borate complexes of Co^{2+}, are also successful relaxation agents as well. The pulsed EPR work reported here on Fe^{2+} suggests that the isoelectronic Co^{3+} would also be suitable as a relaxation reagent in similar low-temperature experiments. However, it is clear that pulsed EPR measurements are needed at fields of ~5 T and higher to adequately characterize the field-dependent behavior of the dopant. A metal center that would *not* be acceptable would be the Cr^{3+}. We performed pulsed EPR and solid-state proton NMR experiments using $Cr(acac)_3$. The $Cr(acac)_3$ provides the required reduction in the ^{1}H T_1's, while reducing the value of $T_{1\rho}$ for the ^{1}H's to be too short to be of any utility in the CP experiment. However, it should be clear that the dopant strategy is not specific to ^{67}Zn NMR. Rather, it is the means to control the relaxation properties of the ^{1}H spin bath that provides the magnetization that is transferred to the spin of interest. Hence, these methods will work equally as well for experiments focused on the chemistry or structure of systems containing the ions Mg^{2+} or Ca^{2+}.

As a successful illustration of this method of managing the ^{1}H relaxation, we have examined the ^{67}Zn NMR of four Zn-poly(pyrazolyl)borates complexes, $[HB(3,5\text{-}Me_2pz)_3]_2Zn$, $[HB(pz)_3]_2Zn$, $[H_2B(3\text{-},5\text{-}Me_2pz)_2]_2Zn$, and $[H_2B(pz)_2]_2Zn$. The octahedral complexes are characterized by modest values of C_q ranging from nominally 4 MHz for $[HB(pz)_3]_2Zn$ to 2.6 and 4.5 MHz for $[HB(3\text{-},5\text{-}Me_2pz)_3]_2Zn$ at low and room temperatures, respectively. For the tetrahedral complexes, the values of C_q are significantly larger with values in the neighborhood of 14−15 MHz. These large values of C_q reflect the relative distortion around the Zn^{2+} in the tetrahedral complexes relative to the octahedral complexes.

A significant point is that the present systems are all soluble in organic solvents. Hence, sample preparation was simple. The sample was prepared by mixing the compound of interest and the dopant in the same solvent and then drying in a convenient manner. Water-soluble systems represent more of a challenge. Ideally, the paramagnetic metal system should be designed in such a way as to be benign to the system of interest. However, preparation of the crystalline sample presents the problem that the dopant and system of interest cannot phase separate during the crystallization procedure. Phase separation will prevent the dopant from having the desired effect on the proton spin system as a whole. In the case of biological systems, the problem is less severe. With these systems, the protein of interest can serve as the ligand for the dopant. This latter procedure has worked well in our protein experiments.[34]

Calculations of the field gradient tensor for these complexes were modestly successful. The trend of increasing values of C_q with decreasing coordination number of the zinc was reproduced by theory. However, the details within a given coordination environment, especially within the tetrahedral complexes, were less successful. The exact origin of this difficulty is yet to be defined. However, the geometry used in these calculations is critical as is the basis set. The basis set employed was at the triple-ξ level, but the geometries employed were those determined by X-ray crystallography and were not optimized. Further, the calculations were performed on single molecules and did not include the next nearest neighbor molecules of the unit cell. It is expected that as basis sets improve, ab initio computational methods will provide needed insights into the structural basis for specific trends in magnetic resonance parameters.

It is clear that the future utilization of low-temperature NMR experiments of the type illustrated here will profit significantly by the use of appropriately chosen relaxation reagents. There is no doubt that such reagents will play a critical role in the enhancement of this methodology as applied to bioinorganic systems. It is also obvious that the structural changes within the poly(pyrazolyl)borate complexes **1**−**4** have clouded our ability to demonstrate the sensitivity of ^{67}Zn quadrupole parameters to specific changes. However, what is clear is that the ^{67}Zn quadrupole parameters are sensitive to all of the changes that occur. Future work will involve investigations of poly(pyrazolyl)borate complexes of the type N_3Zn-X in an effort to examine the possibilities of systematic changes to the framework as a function of X.

Acknowledgment. The authors gratefully acknowledge Drs. Christine Little and Mark Smith of the University of South Carolina for their assistance with the X-ray measurements. The authors would like to further acknowledge several discussions with Professor Niels Nielsen of Aarhus University with respect to details of the SIMPSON program. This work was supported in part by the National Institutes of Health (Federal Grant GM26295) and by the Department of Energy, Office of Biological and Environmental Research Program under grants KP11-01-01: 24931 and 41055. The research was performed in the Environmental Molecular Sciences Laboratory (a national scientific user facility sponsored by the DOE Biological and Environmental Research) located at Pacific Northwest National Laboratory and operated for DOE by Battelle.

JA0127133

(34) Lipton, A. S.; Heck, R. H.; Ellis, P. D., to be submitted.